JMEPEG (2012) 21:530–539
DOI: 10.1007/s11665-011-9943-y

1059-9495/$19.00

Characteristics of Laser Beam and Friction Stir Welded AISI 409M Ferritic Stainless Steel Joints

A.K. Lakshminarayanan and V. Balasubramanian

(Submitted July 6, 2010; in revised form February 1, 2011)

This article presents the comparative evaluation of microstructural features and mechanical properties of friction stir welded (solid-state) and laser beam welded (high energy density fusion welding) AISI 409M grade ferritic stainless steel joints. Optical microscopy, microhardness testing, transverse tensile, and impact tests were performed. The coarse ferrite grains in the base material were changed to fine grains consisting duplex structure of ferrite and martensite due to the rapid cooling rate and high strain induced by severe plastic deformation caused by frictional stirring. On the other hand, columnar dendritic grain structure was observed in fusion zone of laser beam welded joints. Tensile testing indicates overmatching of the weld metal relative to the base metal irrespective of the welding processes used. The LBW joint exhibited superior impact toughness compared to the FSW joint.

Keywords ferritic stainless steel, friction stir welding, impact toughness, laser beam welding, tensile strength

1. Introduction

AISI 409M grade ferritic stainless steels are widely used to construct coal wagons for transporting iron ore. The different parts made from 409M grade are box body (including the inner and outer walls, floor plate, and wagon under-frame), vertical side stanchions, and flab doors (Ref 1). These steels generally conforms in composition to grades S41003 (ASTM A240) and 1.4003 (EN 10088-2 and EN 10028-7). The steel was developed from the ferritic stainless steel AISI 409 by careful balancing of ferrite (Cr, Si, Ti) and austenite (Ni, Mn, C, N) stabilizing elements using Kaltenhauser's relationship (Ref 2) presented in Eq 1

$$\text{Kaltenhauser Ferrite Factor (KFF)} = \text{Cr} + 6\text{Si} + 8\text{Ti} - 2\text{Mn} - 4\text{Ni} - 40(\text{C} + \text{N}) \quad \text{(Eq 1)}$$

The steels under consideration are designed to transform partially to austenite on cooling, passing through the dual-phase austenitic-ferritic phase field on the Fe-Cr equilibrium phase diagram (Fig. 1a). This partial solid-state phase transformation of ferrite to austenite on cooling improves the weldability and as-welded toughness by restricting heat-affected zone (HAZ) grain growth (Ref 3). In high-purity Fe-Cr systems ($C < 0.01$ wt.%), the gamma loop (Fig. 1b) extends as far as about 13.5% Cr, after which the structure is fully ferritic at all temperatures (Ref 4). However, when the carbon content of steel is increased to 0.03% the gamma loop extend to around 20% Cr (Fig. 1b). Due to low alloying content, the steel used in this study lies in the dual phase region, and the structure would therefore consists of a mixture of untransformed delta ferrite, alpha ferrite which transformed from austenite on cooling and martensite, depending on the cooling rate (Ref 5) and that is why it is variously described as "ferritic" or "ferritic-martensitic" 12% Cr stainless steel (Ref 6).

The 409M grade stainless steels are usually supplied in the fully annealed and desensitized condition. Final annealing is performed at temperatures below the A1 (normally between 700 and 750 °C) after air cooling or cold rolling. Though the modified 12% Cr ferritic stainless steels are having better weldability than conventionally used ferritic stainless steels, the steel still suffers from grain growth in the HAZ and fusion zone results in significant alterations in the mechanical properties (Ref 7). Due to the high energy density, laser beam welding is attractive for ferritic stainless steel, because of the narrow width of the fusion zone and HAZ (Ref 8). The general attributes of a laser beam weld are that the relative heat input is low when compared to other welding processes, and therefore the cooling rate is relatively high (Ref 9). The inherent rapid solidification makes the use of lasers very attractive because completed welds contain a range of microstructures with metastable and stable phases, minimum segregation and fine grain sizes which often improve the mechanical properties (Ref 10).

Friction stir welding (FSW) is a novel solid-state joining process that was invented in 1991, it can avoid many problems associated with fusion welding processes, thereby defect-free welds having excellent properties can be produced even in some materials with poor fusion weldability (Ref 11). In recent years, FSW of high melting temperature materials such as steels, nickel, and titanium alloys has become a research hotspot (Ref 12). The main obstacle to use FSW with these higher melting point materials is the development of tool materials capable of surviving the high temperatures and forces generated by the process. Considerable advances have been made, mainly through improved materials selection and tool design (Ref 13-16). Tool material development work has

A.K. Lakshminarayanan and **V. Balasubramanian**, Department of Manufacturing Engineering, Centre for Materials Joining & Research (CEMAJOR), Annamalai University, Annamalai Nagar 608002, Tamil Nadu, India. Contact e-mails: akln2k2@yahoo.com and visvabalu@yahoo.com.

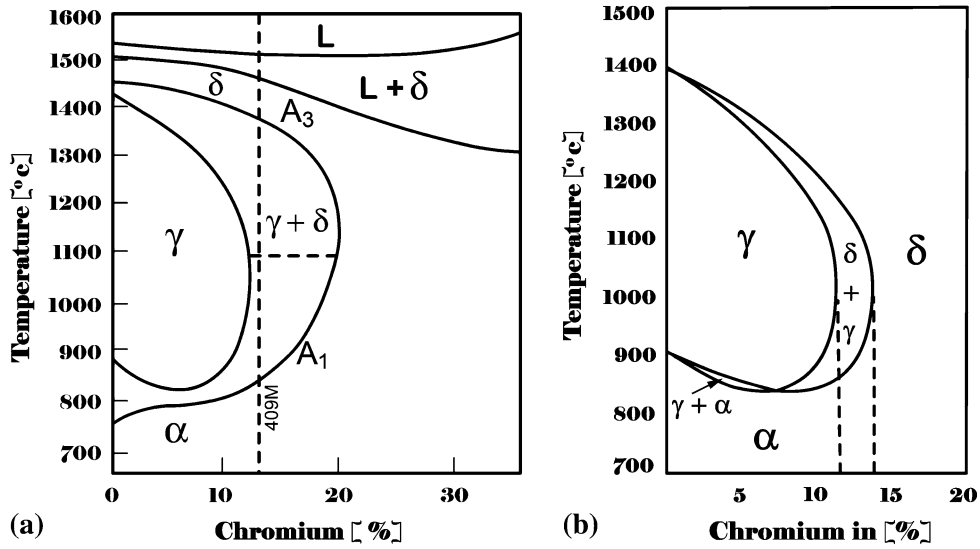

Fig. 1 Fe-Cr equilibrium phase diagram showing the position of 409M ferritic stainless steel. (a) carbon = 0.03 wt.% and (b) carbon < 0.01 wt.%

Table 1 Chemical composition (wt.%) of base metal

C	Cr	Ni	Nb	Cu	Si	Mn	P	S	N	Al	Co	Ti	V	Fe
0.028	11.00	0.4	0.009	0.365	0.45	1.15	0.4	0.16	0.04	0.01	0.2	0.008	0.017	Bal

looked primarily at refractory metals (e.g., W-Re) (Ref 13), polycrystalline boron nitride (PCBN) (Ref 14), and WC (Ref 15, 16).

FSW of ferritic stainless steels can lead to improvement in mechanical properties by microstructural refinement compared to the fusion welding processes (Ref 17, 18). Characteristics of ferritic stainless steel joints fabricated by traditional arc welding processes have been examined by several researchers (Ref 19-22). However, details on high energy density processes such as laser beam (LB) welding of ferritic stainless steel are scarce. Moreover, details of microstructure and mechanical properties of laser beam welded 409M grade ferritic stainless steels and comparison with a friction stir welding process is not yet reported in literature. In this investigation, microstructure analysis, microhardness survey, tensile and impact toughness tests were carried out to evaluate the joint performance and the weld zone characteristics of FSW and LBW joints of 409M grade ferritic stainless steel and the results are presented in this article.

2. Experimental

The as-received base material used in this study was 4 mm thick cold rolled, annealed, and pickled AISI 409M grade ferritic stainless steel plate. The chemical composition of the base metal presented in Table 1 was obtained using a vacuum spectrometer (ARL, model 3460). Sparks were ignited at various locations, and their spectrum was analyzed for the estimation of alloying elements. Square butt joints were fabricated autogenously (without filler metal addition) using LBW and FSW processes. Full penetration friction stir welded and laser beam welded joints were made perpendicular to the rolling direction of the plates (75 × 150 mm). An indigenously designed and developed CNC controlled friction stir welding machine (6 Ton, 4000 rpm, 22 kW) was used in position control mode to fabricate the FSW joint. Laser beam welding was carried out using 3.5 kW CO_2 laser welding system (Make: Rofin, Germany; Model: #DC-035). Few welding trials were carried out and specimens were extracted from various locations of the joint and subjected to macrostructural analysis. The specimen free of volumetric defect and lack of penetration was considered as the optimized welding condition. Also care was taken to avoid the FSW tool pin failure and control the heat input by controlling the combination of tool rotational speed and welding speed. The welding conditions and optimized process parameters presented in Table 2 were used to fabricate the joints for further investigation. The photograph of fabricated FSW and LBW joints are displayed in Fig. 2. The welded joints were sliced (as shown in Fig. 3) using abrasive cutting and then machined to the required dimensions for preparing tensile, impact test, and metallographic specimens.

Two different tensile specimens were prepared as shown in Fig. 4(a) and (b) to evaluate the transverse tensile properties. Un-notched smooth tensile specimens were prepared to evaluate the transverse tensile properties of the joints such as yield strength, tensile strength, and elongation. Notched specimens were prepared to evaluate notch tensile strength and notch strength ratio (notched tensile strength/un-notched tensile strength) of the joints. Flat micro-tensile longitudinal specimens (Fig. 4c) were prepared to characterize the tensile properties of all weld metal of FSW and LBW joints. Three samples were tested to consider repeatability that cannot minimize errors, but

one can realize variability. Tensile testing was carried out using 100 kN electromechanical controlled universal testing machine (FIE-Blue Star, India; model UNITEK-94100). ASTM E8M-04 guidelines (Ref 23) were followed for preparing and testing the tensile specimens.

Charpy impact specimens were prepared to the dimensions shown in Fig. 4(d) and (e) to evaluate the impact toughness of the weld metal and HAZ, and hence the notch was placed (machined) at the weld metal (weld center) as well as in the HAZ. As the plate thickness is small, subsized specimens were prepared. Impact testing was conducted at room temperature using a pendulum-type impact testing machine (ENKAY, India) with a maximum capacity of 300 J. The amount of energy absorbed in fracture was recorded, and the absorbed energy is defined as the impact toughness of the material. ASTM E23-04 specifications (Ref 24) were followed for preparing and testing the impact specimens.

A Vickers microhardness testing machine (Shimadzu, Japan; model: HMV-2T) was used for measuring the hardness of the weld with 0.05 kg load and 15 s. Microstructural examination was carried out using optical microscope (MEJI, Japan; model: MIL-7100) incorporating metal vision image analyzing software. The specimens for metallographic examination were sectioned to the required size from the joint comprising weld metal, HAZ, and base metal regions, and polished using different grades of emery papers. Final polishing was done using a diamond compound (2 μm particle size) in the disc polishing machine. The specimens were etched with standard Vilella's reagent (Ref 25) for 30 s. Ferrite content of the weld metal was calculated and predicted by chemical analysis results, then was determined by Ferritescope (Fisher; model: mp30) measurements across the weld metal. The fractured surface of the tensile and impact tested specimens was analyzed using a scanning electron microscope (JEOL, Japan; model: 6410LV) at higher magnification to study the fracture morphology and establish the nature of the fracture.

XRD analysis was carried out in Theta-Theta (Vertical type), D/Max (Make: RIGAKU, Japan; Model: ULTIMA-III) with copper target under a working voltage of 40 kV and 40 mA working current. Scintillation counter detector was used with a scan range 3° to 154° (min. setup size 0.0002°). A qualitative analysis of the precipitate was carried out by x-ray diffraction based on the identification of the peaks after refinement, using PROFIT and PCPDFWIN software to adjust the exact peak angular position of the phases presented in the weld metal of FSW and LBW joints. Based on the values of the peaks in the diffractograms, a comparison with JCPDS card values was made, to identify the phases, which could precipitate in the 409M ferritic stainless steel.

Table 2 Welding conditions

	Process	
Parameters	**LBW**	**FSW**
Welding machine	Rofin, Germany	RV Machine Tools, India
Power, kW	3.5	…
Focal length, mm	300	…
Focal spot diameter, μm	180	…
Shielding gas, L/min	30	…
Welding speed, mm/min	3000	50
Tool rotational speed, rpm	…	1000
Axial force, kN	…	33.5
Tool material composition	…	W 90%, Ni 3%, Mo 1%, Co 1%, Fe bal
Tool pin profile	…	Taper cylindrical
Shoulder diameter, mm	…	20
Pin diameter, mm	…	Tapered from 8 to 5
Pin length, mm	…	3.7

3. Results

3.1 Macrostructure

The cross-sectional macrostructure of the FSW and LBW joints is shown in Fig. 5. No volumetric defect is observed. The macrostructure of the LBW joint consists of four different regions such as fusion zone or weld metal region, high-temperature HAZ (HTHAZ), low-temperature HAZ (LTHAZ), and the base metal (BM). Similarly, the macrostructure of FSW joint consists of stir zone (SZ), a region either side of the stir zone, which can be termed as the thermo-mechanically affected zone (TMAZ), inner HAZ (IHAZ), outer HAZ (OHAZ), and the base metal (BM) region.

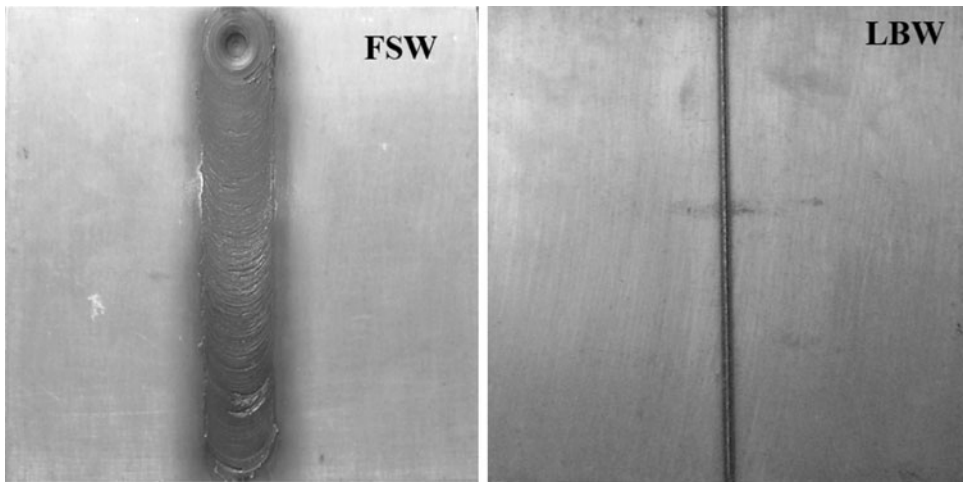

Fig. 2 Fabricated joints of 409M ferritic stainless steel

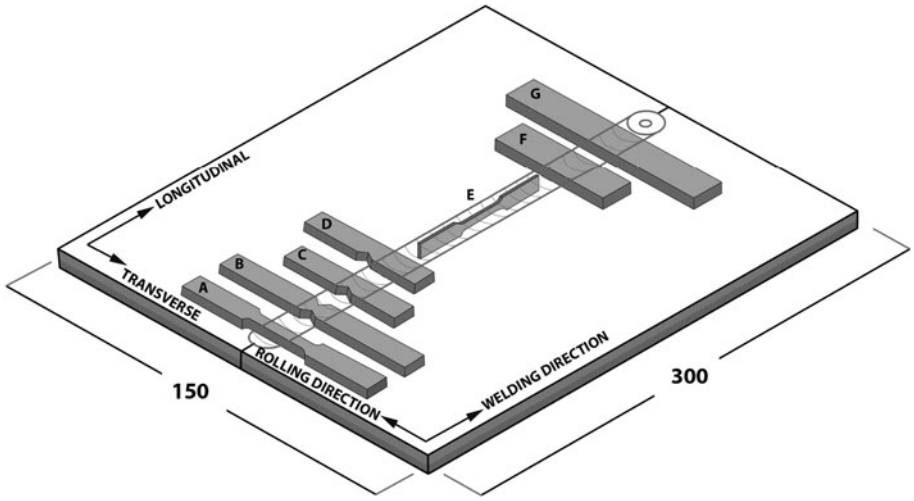

Fig. 3 Scheme of extraction of specimens for mechanical testing (A—smooth tensile specimen, B—notched tensile specimen, C and D—impact specimen notch placed at the weld center and HAZ respectively, E—longitudinal flat micro tensile specimen, F and G—metallographic specimen)

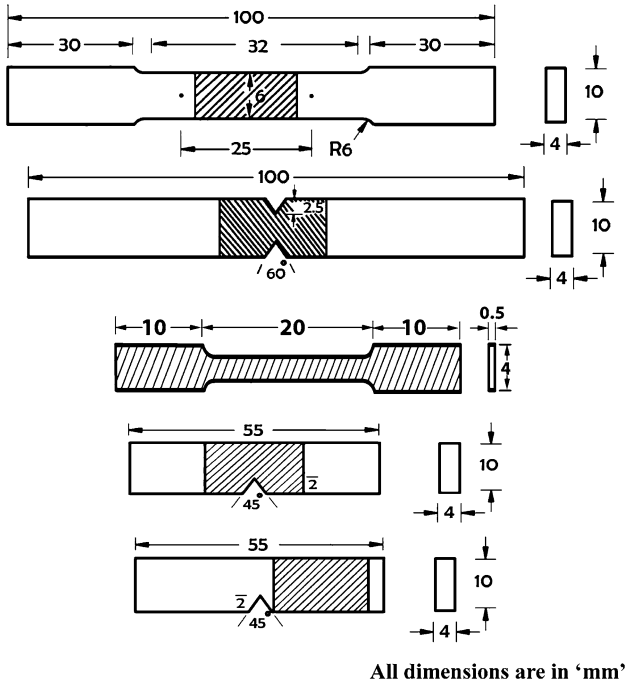

Fig. 4 Dimension of specimens for mechanical testing

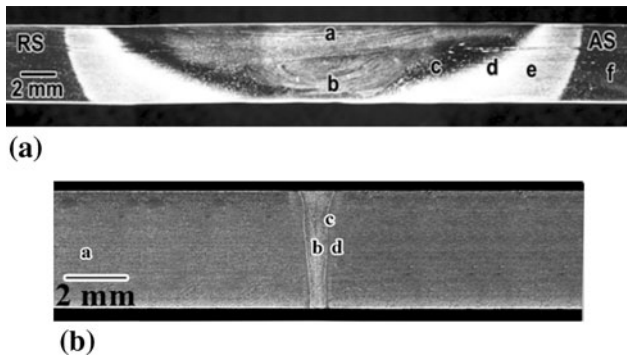

Fig. 5 Macrostructure of friction stir and laser beam welded 409 M ferritic stainless steel. (a) FSW [a—flow arm: shoulder influenced region, b—banded structure: pin influenced region, c—thermo mechanical affected zone, d—inner heat affected zone (IHAZ), e—outer heat affected zone (OHAZ), AS—advancing side, RS—retreating side, f—base metal (BM)]. (b) LBW [a—base metal, b—fusion zone (FZ), c—high temperature heat affected zone (HTHAZ), d—low-temperature heat affected zone (LTHAZ)]

3.2 Tensile Properties

In each condition, three tensile specimens were tested; the mean and standard deviation of the three results are presented in Table 3. The higher yield strength, higher tensile strength, and lower elongation of FSW and LBW joint are observed compared to the base metal (Fig. 6). Joint efficiency is the ratio between tensile strength of welded joint and tensile strength of the unwelded parent metal. Both FSW and LBW joints exhibited 100% joint efficiency as the failure took place in the base metal region. Notch tensile strength of the friction stir welded joint is 1030 MPa, which is 34% higher than the LBW joint. The fracture elongation of friction stir welded and laser beam welded 409M joints are 6 and 4% higher respectively compared with the base metal. Since the transverse tensile specimens fractured in the base metal region (Fig. 7), flat micro-tensile specimens were prepared to characterize the tensile properties of the all weld metal of FSW and LBW joints and the results are presented in Table 3.

3.3 Impact Toughness

Charpy impact toughness of the FSW and LBW joints were evaluated and presented in Table 3. The impact toughness of unwelded base metal is 34 J. The impact toughness of FSW joint with notch placed at the weld centerline and HAZ region are 28 and 30 J, respectively, which are 25 and 3% lower when compared to the weld metal and HAZ toughness of LBW joints.

3.4 Hardness and Microstructure

The micro-hardness profile of FSW and LBW joints of 409M ferritic stainless steel is presented in Fig. 8. The hardness

Table 3 Tensile and impact properties of FSW and LBW joints

Joint	Yield strength, MPa	Tensile strength, MPa	Elongation, %	Notch tensile strength, MPa	Notch strength ratio, NSR	Impact toughness, J	
						WM	HAZ
BM	364 (4.32)	536 (5.12)	31 (1.15)	662 (3.54)	1.24	34 (0.96)	
FSW joint	382 (5.18)	574 (6.42)	33 (0.931)	1030 (1.10)	1.79	28 (1.51)	30 (0.81)
FSW (all weld)	612 (6.40)	910 (2.11)	26 (1.04)	…	…	…	…
LBW joint	382 (4.3)	546 (2.9)	32 (1.3)	764 (4.6)	1.34	35 (1.8)	31 (2.5)
LBW (all weld)	412 (2.1)	704 (3.1)	29 (0.8)	…	…	…	…

Values given in the brackets are standard deviation of experimental result

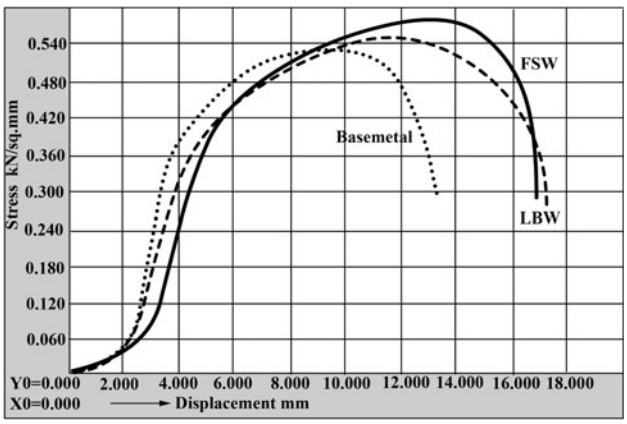

Fig. 6 Load displacement curves recorded during tensile testing

Fig. 7 Fracture location of tensile specimens. (a) FSW and (b) LBW

of the as-received base metal is approximately 170 HV0.05. The hardness at the mid cross section of FSW joint varies from 320 to 380 HV0.05, depending on the grain size and phases sampled by each indentation. Similarly, the hardness at the mid cross section of FSW joint varies from 290 to 325 HV0.05, depending on the grain size and phases sampled by each indentation. The base metal exhibits a microstructure of ferrite grains approximately 30 μm in diameter with randomly distributed carbides (Fig. 9a). The laser beam weld metal consisted largely of columnar dendritic grains formed by epitaxial growth, as shown in Fig. 9(e). LB welds contain columnar grains at the outer portion with equiaxed axial grains in the central regions (Fig. 9b, c). Very fine equiaxed ferrite

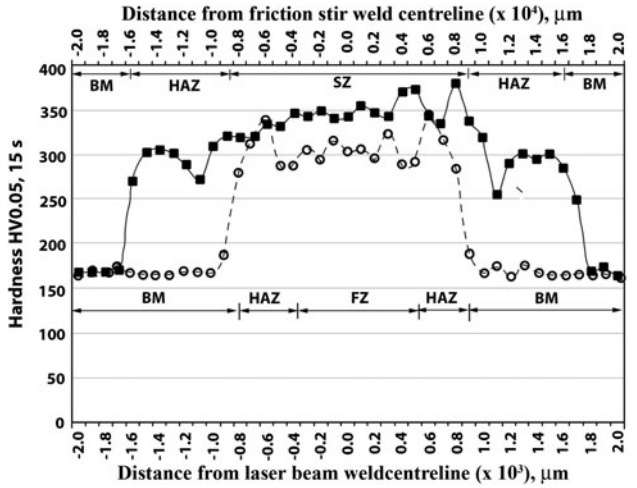

Fig. 8 Hardness profile of LBW and FSW joints of 409M ferritic stainless steel

grains with grain boundary martensite of 4 μm are observed at the top of the stir zone (Fig. 10b), whereas semi-elliptical banded structure of ferrite and martensite is observed in the bottom region of the stir zone (Fig. 10c). In the TMAZ, a distorted structure with grains re-oriented perpendicular to the transverse direction is observed (Fig. 10d, e). It should be noted that the TMAZ/SZ boundary on the advancing side (Fig. 10e) of the tool is sharper than that on the retreating side (Fig. 10d). The IHAZ was observed to be similar to the base metal with grain boundary martensite, whereas the microstructure of the OHAZ consisted of finer equiaxed grains (Fig. 10f).

3.5 Fracture Surface

The fracture surface of tensile and impact toughness tested specimens of welded joints was analyzed using SEM to reveal the fracture surface morphology. Figure 11 displays the fractographs of tensile and impact specimens. The fractographs of tensile and impact specimens show ductile fracture (presence of dimples) irrespective of welding processes used.

3.6 X-ray Diffraction Analysis

Figure 12 shows the x-ray diffraction pattern for base metal, weld metal of FSW and LBW joint. The presence of larger peaks corresponding to ferrite (α) and peaks of smaller intensity, which correspond to the precipitates, can be seen. The XRD results of base metal (Fig. 12a) indicated the

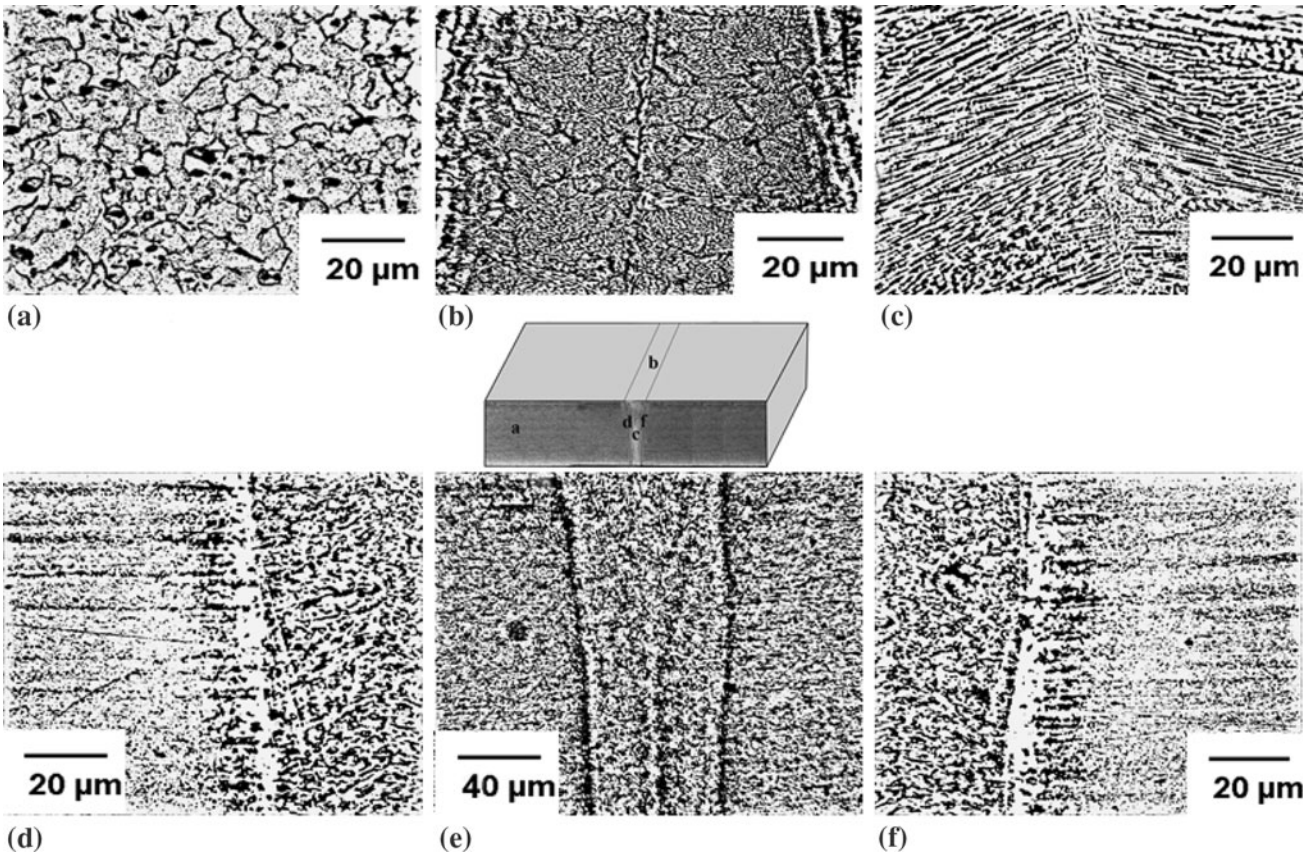

Fig. 9 Optical micrographs of laser beam welded 409M ferritic stainless steel joint. (a) Base metal, (b) fusion zone top region, (c) fusion zone cross section middle, (d) interface left side, (e) joint cross section, (f) interface right side

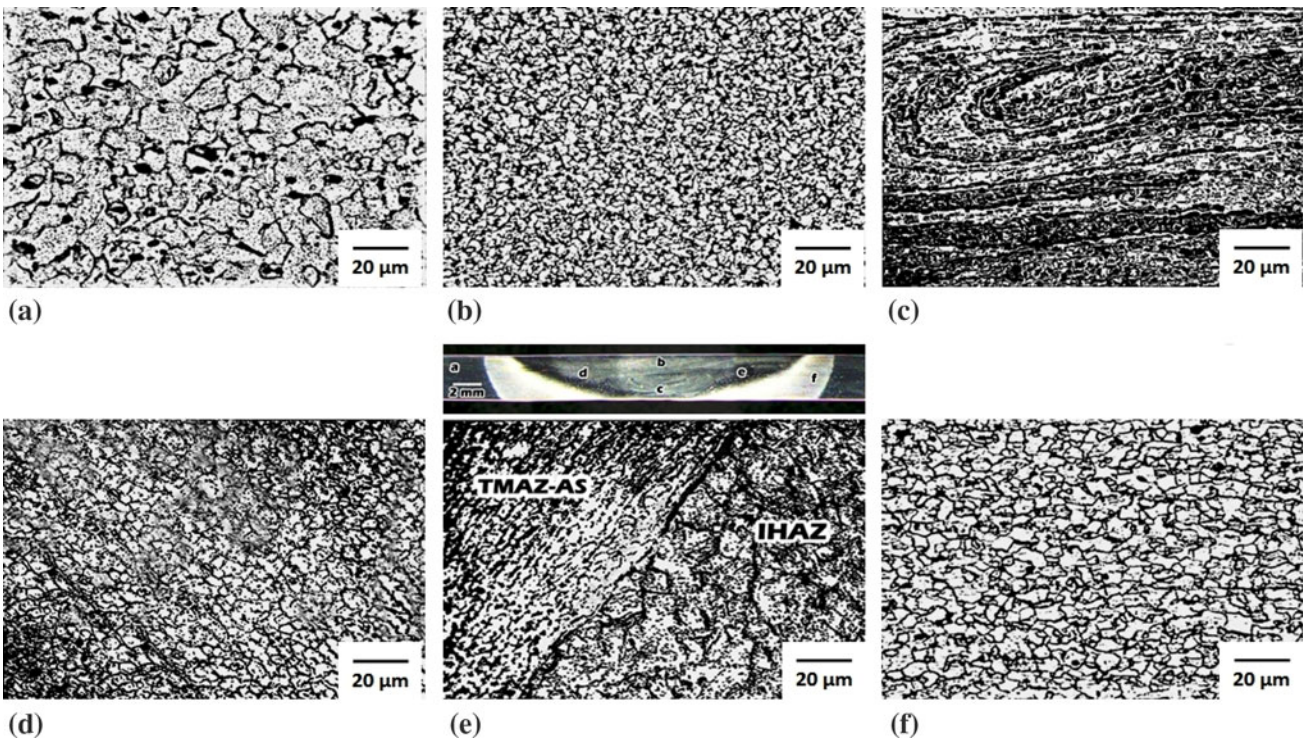

Fig. 10 Optical micrographs of friction stir welded 409M ferritic stainless steel joints. (a) Base metal, (b) stir zone—shoulder influenced region, (c) stir zone—pin influenced region, (d) thermo-mechanically affected zone-retreating side (TMAZ-RS), (e) thermo-mechanically affected zone-advancing side, (f) outer heat affected zone

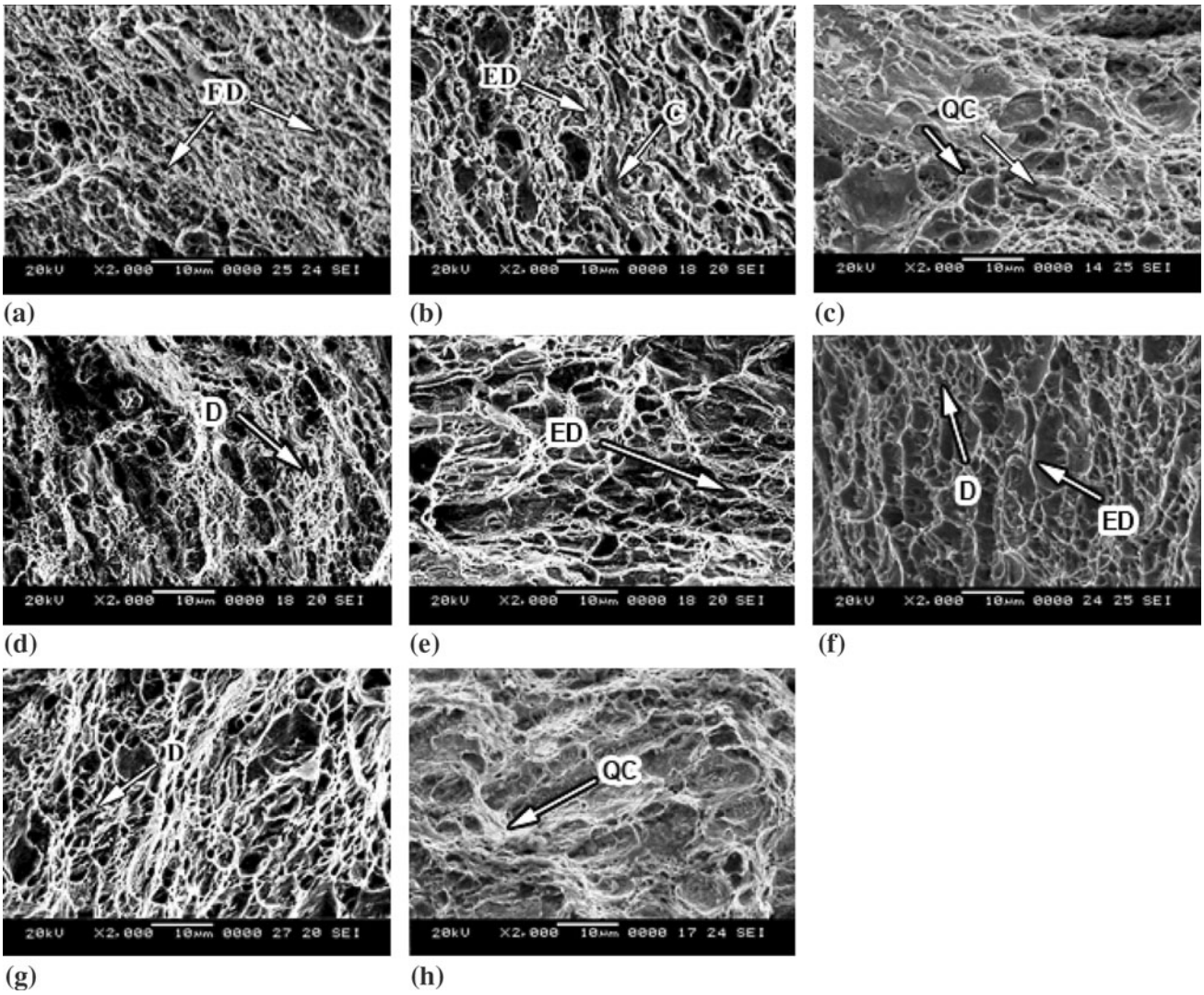

Fig. 11 SEM fractographs of tensile and impact specimens. (a) FSW tensile—all weld, (b) FSW impact—WM, (c) FSW impact—HAZ, (d) LBW tensile, (e) LBW impact—WM, (f) LBW impact—HAZ, (g) base metal tensile, (h) base metal impact. D, dimples; FD, fine dimples; ED, elongated dimples; QC, quasi cleavage

presence of ferrite (α) and $Cr_{23}C_6$ carbides. However, the diffractograms of weld metal region (Fig. 12b, c) indicate the presence of ferrite (α), martensite, and carbides. Through the diffractograms, it is possible to confirm the presence of $Cr_{23}C_6$ carbides in LBW joint. However, XRD results indicate the probable presence of $Cr_{23}C_6$ and Fe_6W_6C carbides in the weld metal region of FSW joint.

4. Discussion

Transverse tensile properties of the base metal and welded joint are presented in Table 3. The weld metal region has the higher ultimate tensile strength (UTS) and 0.2% offset yield strength (YS), and lower elongation than the BM. The tensile specimen of the weld fractured in the BM region, because the BM had the lowest hardness in the present weld, as shown in Fig. 7 and 8. The strength is roughly proportional to hardness, so that the BM region would preferentially yield and then fail during transverse tensile test. Flat micro-tensile specimens were used to determine the tensile properties of the weld metal of the laser beam weld. Substantial differences in strength properties (mismatching) of the base metal and narrow fusion zone of the LB welds inevitably occur due to the rapid thermal cycle of the joining process. The overall mechanical properties of a weld are determined by the characteristic properties of the individual microstructures present in the weld zone and the HAZ of LBW joint.

The fusion zone of the laser beam weld consists of columnar grains and axial grains (Fig. 9b, e). The thermal conductivity of ferritic stainless steel is being higher; the heat flow in the direction perpendicular to the weld would be maximum. Therefore, the grains tend to grow in that direction, giving rise to columnar grains. The columnar dendritic structure of the grains observed on the ferritic stainless steel is in conformity with general trends reported for such welds (Ref 26, 27). Axial grains initiate in the original weld bead and grow along the length of the weld, blocking the columnar grains growing in from the fusion lines. Axial grains observed in laser beam

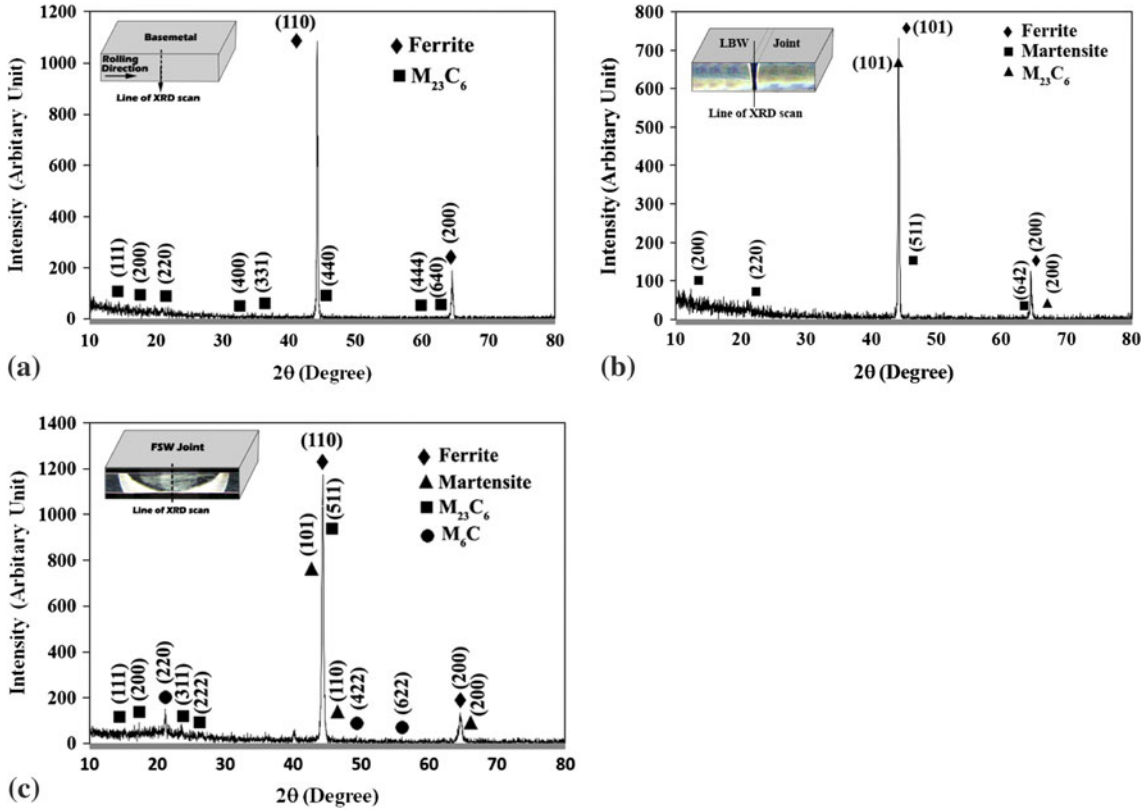

Fig. 12 X-ray diffraction pattern for (a) base metal, (b) LBW, (c) and FSW joints

welds are due to the fact that this is the last region to solidify, and this type of grain structure is consistent with trends reported in welds (Ref 28).

When considering a weld cross section, each point at a given distance from the weld center line experiences a different peak temperature and cooling rate. As the distance from the weld center line increases, the peak temperature and cooling rate decrease and this influences the microstructure that develops (Ref 29). The fusion zone and HTHAZ (heated above about 1300 °C) reaches the δ ferrite range and considerable grain growth takes place at high temperatures in case of conventional arc welding. However, a characteristic feature of the laser beam 409M ferritic stainless steel welds was the virtual absence of grain growth in the HAZ. The problem of extensive grain coarsening and associated brittleness often cited in the welding of ferritic stainless steels by arc processes is essentially absent from laser beam welding process. The grain size in the HTHAZ of the LB welds was found to be very similar to that of the BM with low carbon grain boundary martensite. This phenomenon is due to the relatively low heat input associated with laser beam welding. During cooling through the austenite formation ranges, a considerable amount of austenite formed at the grain boundaries, which are determined by the relative amount of ferrite and austenitic stabilizing elements and the cooling rate. If the cooling rate is not excessive, the austenite has time to grow and cover all available ferrite grain boundaries. However, under the rapid cooling rates associated with LBW, transformation to austenite was fairly suppressed leading to a predominantly ferritic structure accompanied with continuous networks of martensite along the grain boundaries. The steel used in this study is not sufficiently alloyed for the austenite to remain stable down to room temperature, therefore, it transforms to low carbon lath martensite. It has been found that when levels of ferrite are increased, there is less austenite available at high temperature for the solution of carbon which can lead to chromium carbide precipitation. A much wider duplex zone with tough fine grained ferrite and low carbon lath martensite right next to coarse grained zone (Fig. 9d, f) was observed. This wider low-temperature heat affected duplex zone originated when the material was heated to temperatures (900-1300 °C) within the dual phase ferrite and austenite phase field. The maximum amount of martensite formed at the point in this zone at which the longest time was spent during welding and at the temperature of 1050 °C at which the maximum amount of austenite will form. The presence of hard untempered martensite would reduce the ductility of the weld and could act as stress raisers and crack initiation points (Ref 30). However, one of problems plaguing ferritic stainless steels is rapid grain growth at high temperature with subsequent brittleness, and substantial transformation of austenite and martensite during cooling will result in significant grain refinement and improvement in toughness (Ref 31). Since weld microstructure is greatly influenced by chemical composition, the chromium equivalent and nickel equivalent based on Balmforth and Lippold constitutional diagram (Ref 32) for ferritic-martensitic stainless steel are calculated by using the Eq 2 and 3.

$$Cr_{Eq} = Cr + 2Mo + 10(Al + Ti) \quad \text{(Eq 2)}$$

$$Ni_{Eq} = Ni + 35C + 20N \quad \text{(Eq 3)}$$

By plotting Cr_{Eq} and Ni_{Eq} values on the constitution diagram, approximately 80% ferrite and 20% martensite is

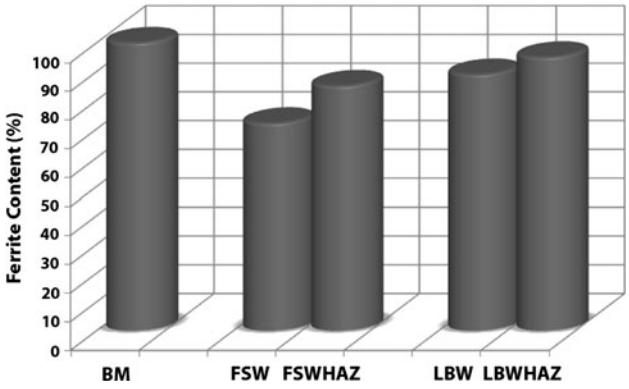

Fig. 13 Weld metal ferrite content analysis of the LBW and FSW weldments

expected in the weld metal. Ferrite content of the weld metal of the samples prepared from LBW joints was measured by Fisher Ferritescope and the data are presented in Fig. 13. As seen from the Fig. 13, almost 90% ferrite was measured on the weld metals, the values are close to the predicted value of approx. 80% ferrite. Grain refinement of ferritic stainless steel weldments will substantially increase the tensile and impact properties (Ref 33). The grain sizes of the LB-weld metal and HAZ were finer than those of the BM as a result of characteristic epitaxial solidification. The better strength and toughness of 409M laser beam welds could be due to a fine solidification structure as a result of fast solidification and is due to a combination of equiaxed and columnar grain perpendicular to the crack path.

Microstructure observation on the FSW specimens suggests that the top region of the stir zone shows very fine equiaxed grains of ferrite and martensite (Fig. 10b). Workpiece material closest to the tool shoulder experiences greater strain relative to material away from the shoulder, resulting in refinement in the top of the stir zone. The bottom region (Fig. 10c) shows the banded appearance of ferrite and martensite with some very tiny particles of tungsten-enriched carbides. It is well accepted that generation of fine and equiaxed grains in the SZ is a result of dynamic recrystallization due to the friction heat between the tool and workpiece during friction stir welding (Ref 34). Dynamic recrystallization may occur discontinuously by nucleation of new grains and growth by motion of high angle grain boundaries or continuously by increasing misorientation of existing sub grain boundaries due to absorption of dislocations (Ref 35). Materials with low stacking fault energy (SFE) such as austenitic stainless steels generally undergo discontinuous dynamic recrystallization. Whereas, materials with high SFE such as ferritic stainless steels tends to undergo continuous dynamic recrystallization (Ref 36). According to the phase diagram (Fig. 1a), the stir zone heated at 1250 °C would show duplex microstructure of ferrite and austenite during FSW. The austenite phase would be nucleated along the grain boundary of ferrite during heating cycle. The duplex microstructure of ferrite and austenite experiences both frictional heating and severe plastic deformation caused by rotating welding tool during FSW. It is interesting to note that ferrite experiences dynamic recrystallization more easily than austenite in duplex microstructure, because soft ferrite can absorb more strain energy than hard austenite and reduce it through the relieving process of the strain. These reasons suggest that the SZ has dynamically recrystallized grain structure of ferrite and austenite at elevated temperatures during FSW. The austenite formed during heating cycle transforms to ferrite during cooling cycle. However, rapid cooling rate, large strain induced during FSW would prevent transformation of austenite to ferrite and lead to martensite in the stir zone.

The notch tensile strength and notch strength ratio of FSW joint were significantly higher when compared to the base metal and LBW joint and the reason for this could be attributed to the very fine dual-phase microstructure which is characterized by the presence of a second phase (relatively harder martensite phase) in a ferritic soft matrix (Ref 37). This microstructural configuration influences the stress/strain behavior of the material by work hardening due to the plastic deformation. The yield strength is determined by the onset of plastic flow in the soft phase, i.e., ferrite. At this stage the hard phase is still in the elastic region. Also, a dual-phase microstructure acts beneficially in improving the impact toughness. It is interesting to note that Hayden and Floreen (Ref 38) and Wright and Wood (Ref 39) have shown that duplex ferrite-martensitic microstructures-based Fe-Cr-Ni and Fe-Cr-Mn systems, respectively, have superior impact toughness properties relative to either full ferritic or fully martensitic steels of similar composition. The XRD results (Fig.12b) indicate the presence of Fe_6W_6C carbides, which essentially precipitated due the tool wear caused by high temperature and forces acting on the tungsten alloy tool during friction stirring. The tool debris (Fe_6W_6C carbides) in the stir zone resulted in reduction of impact toughness of friction stir welded joint compared to the base metal and LBW joint. However, superior tensile properties of FSW joint over LBW joint, results from the synergetic effect of the low carbon lath martensite and the fine grain structure.

5. Conclusions

The microstructure and mechanical properties of laser beam and friction stir welded AISI 409M ferritic stainless steel joints were investigated. From this investigation the following important findings are derived:

- The coarse ferrite grains in the base material are changed to fine columnar dendritic grains and equiaxed axial grains of ferrite with some grain boundary lath martensite as a result of characteristic epitaxial solidification of laser beam.
- The coarse ferrite grains in the base material are changed to very fine duplex structure of ferrite and martensite due to the rapid cooling rate and high strain induced by severe plastic deformation caused by frictional stirring.
- Tensile strength of friction stir weld metal is found to be 22 and 41% higher, respectively, compared to the tensile strength of laser beam weld metal and base metal.
- The hardness of the fusion zone in LBW joint is varying from 290 to 325 HV, whereas, the hardness of the stir zone in FSW joint is varying from 320 to 382 HV, which are higher than the base material hardness (170 HV).
- The joints fabricated by LBW process exhibit higher weld metal and HAZ impact toughness values and the enhancement in toughness is approximately 25 and 3% compared to the weld metal and HAZ of FSW. It is due to the presence of equiaxed and columnar dendritic grains perpendicular to

the crack path. Inclusion of tungsten in the pin influenced region resulted in the reduction of ductility and impact toughness of FSW joint compared to the LBW joint.

Acknowledgments

The authors are grateful to Dr. G. Padmanbam, Scientist 'F' and Mr. N. Shanmugarajan, Scientist 'D' of Centre for Laser Processing of Materials (CLPM), International Advanced Research Centre for powder metallurgy & New materials, Hyderabad 500 005, Andhra Pradesh, India for their support and guidance in fabricating LBW joints.

References

1. AISI 409M—Technical Data. 2004. Detail brochure published by SAIL, India
2. R.H. Kalthauser, Improving the Engineering Properties of Stainless Steels, *Source Book on the Ferritic Stainless Steel*, ASM Engineering Bookshelf, American Society for Metals, 1982, p 212–218
3. M. Du Toit and J. Naude, The Influence of Stabilization with Titanium on the Heat Affected Zone Sensitization of 11 to 12% Chromium Ferritic Stainless Steels Under Low Heat Input Welding Conditions, 2009, IIW Doc. IX-H-705-09, p 1–12
4. E. Taban, E. Deleu, A. Dhooge, and E. Kaluc, Laser Welding of Modified 12% Cr Stainless Steel: Strength, Fatigue, Toughness, Microstructure and Corrosion Properties, *Mater. Des.*, 2009, **30**, p 1193–1200
5. M.L.Greef, "The Influence of Welding Parameters on the Sensitisation Behaviour of 3CR12," M.S. Thesis, University of Pretoria, 2006
6. M. Van Warmelo, D. Nolan, and J. Norrish, Mitigation of Sensitisation Effects in Unstabilised 12% Cr Ferritic Stainless Steel Welds, *Mater. Sci. Eng. A*, 2007, **464**, p 157–169
7. A.M. Meyer, "Interstitial Diffusion from the Weld Metal into the High Temperature Heat Affected Zone in 11–12 Percent Chromium Steel Welded Joints," ME Thesis. University of Pretoria, South Africa, 2000
8. M. Penasa and C. Rivela, Application of the Laser Welding Process to Low Thickness Stainless Steels, *Weld. Int.*, 2003, **17**, p 947–957
9. H. Lee and J.L. Wu, The Effects of Peak Temperature and Cooling Rate on the Susceptibility to Intergranular Corrosion of Alloy 690 by Laser Beam and Gas Tungsten Arc Welding, *Corros. Sci.*, 2009, **51**, p 439–445
10. J. Kell, J.R. Tyrer, R.L. Higginson, and R.C. Thomson, Microstructural Characterization of Autogenous Laser Welds on 316L Stainless Steel Using EBSD and EDS, *J. Microsc.*, 2005, **217**, p 167–173
11. W.M. Thomas, E.D.Nicholas, J.C. NeedHam, M.G. Murch, P. Templesmith, and C.J. Dawes. Friction Stir Welding. International Patent Application No. PCT/GB92102203 and Great Britain Patent Application No. 9125978; 1991
12. L. Zhou, H.J. Liu, and Q.W. Liu, Microstructural Characteristics and Mechanical Properties of Friction Stir Welded Joints of Ti–6Al–4V Titanium Alloy, *Mater. Des.*, 2010, **31**, p 2631–2636
13. S. Packer, T. Nelson, C.D. Sorensen, R. Steel, and M. Matsunaga. Tool and Equipment Requirements for Friction Stir Welding Ferrous and Other High Melting Temperature Alloys, *4th Int Friction Stir Welding Symp*, Park City, Utah, USA, in CD-ROM, 2003 (not paginated)
14. C.D. Sorensen, T.W. Nelson, and S.M. Packer, Tool Material Testing for FSW of High-Temperature Alloys, *Proceedings of the Third International Symposium on Friction Stir Welding*, Sept 2001 (Kobe, Japan), TWI, paper on CD
15. A.P. Reynolds, W. Tang, M. Posada, and J. Deloach, Friction Stir Welding of DH36 Steel, *Sci. Technol. Weld. Join.*, 2003, **8**, p 455–460
16. M. Collier, R. Steel, T. Nelson, C. Sorensen, and S. Packer, Grade Development of Polycrystalline Cubic Boron Nitride for Friction Stir Processing of Ferrous Alloys, *Mater. Sci. Forum*, 2003, **426–432**, p 3011–3016
17. S.H.C. Park, T. Kumagai, Y.S. Sato YS, H. Kokawa, K.Okamoto, S. Hirano, and M. Inagaki, Microstructure and Mechanical Properties of Friction Stir Welded 430 Stainless Steel, *Proceedings of The Fifteenth (2005) International Offshore and Polar Engineering Conference*, Seoul, Korea, June 19-24, 2005
18. A.K. Lakshminarayanan and V. Balasubramanian, An assessment of Microstructure Hardness, Tensile and Impact Strength of Friction Stir Welded Ferritic Stainless Steel Joints, *Mater. Des.*, 2010, **31**, p 4592–4600
19. L. Wanga, C.J. Song, F.M. Sun, L.J. Li, and Q.J. Zhai, Microstructure and Mechanical Properties of 12 wt.% Cr Ferritic Stainless Steel with Ti and Nb Dual Stabilization, *Mater. Des.*, 2009, **30**, p 49–56
20. C. Meadows and J.D. Fritz, Understanding Stainless Steel Heat Affected Zones, *Weld. J.*, 2005, **84**, p 25–30
21. K. Shanmugam, A.K. Lakshminarayanan, and V. Balasubramanian, Tensile and Impact Properties of Shielded Metal Arc Welded Ferritic Stainless Steel Joints, *J. Mater. Sci. Technol.*, 2009, **45**, p 181–186
22. E. Taban, E. Deleu, A. Dhooge, and E. Kaluc, Gas Metal Arc Welding of Modified X2CrNi12 Ferritic Stainless Steel Kovove, *Mater. Metall. Mater.*, 2007, **45**, p 67–73
23. ASTM International Standard E8M-04, Standard Test Methods for Tension Testing of Metallic Materials
24. ASTM International Standard E23-06, Standard Test Methods for Notched Bar Impact Testing of Metallic Materials
25. ASTM International Standard E 407-99 Standard Practices for Microetching Metals and Alloys
26. M. Tullmin, F.P.A. Robinson, C.A.O. Henning, A. Strauss, and J.L. Grange, Properties of Laser-Welded and Electron-Beam Welded Ferritic Stainless Steel, *Johannesb. S. Afr. Inst. Min. Metall.*, 1989, **89**, p 243–249
27. G. Madhusudan Reddy and K. Srinivasa Rao, Microstructure and Mechanical Properties of Similar and Dissimilar Stainless Steel Electron Beam and Friction Welds, *Int. J. Adv. Manuf. Technol.*, 2009, **45**, p 875–888
28. R. Kaul, P. Ganesh, A.K. Nath, P. Triapthi, and R.V. Nandedkar, Characterization and Comparison of Laser and Gas Tungsten Arc Weldments of AISI, 430 Stainless Steel, *Met. Mater. Process.*, 2002, **14**(1), p 41–48
29. R.G. Campbell, Ferritic Stainless Steel Welding Metallurgy, *Eng. Mater.*, 1992, **69**(70), p 167–216
30. J.J. Demo, *Structure and Constitution of Wrought Ferritic Stainless Steels in Handbook of Stainless Steels*, D. Peckner and I.M. Benstein, Ed., McGraw-Hill Book Company, New York, 1977, p 5.1–5.40
31. J.C. Lippold and D.J. Kotecki, *Welding Metallurgy and Weldability of Stainless Steels*, Wiley, Hoboken, NJ, 2005
32. M.C. Balmforth and J.C. Lippold, A New Ferritic–Martensitic Stainless Steel Constitution Diagram, *Weld. J.*, 2000, **77**, p 1s–7s
33. G. Madhusudhan Reddy and T. Mohandas, Explorative Studies on Grain Refinement of Ferritic Stainless Steel Welds, *J. Mater. Sci. Lett.*, 2001, **20**, p 721–723
34. S.J. Hales and T.R. McNelley, Microstructural Evolution by Continuous Recrystallization in a Superplastic Al–Mg Alloy, *Acta Metall.*, 1988, **36**, p 1229–1239
35. K.V. Jata and S.L. Semiatin, Continuous Dynamic Recrystallization During Friction Stir Welding of High Strength Aluminum Alloys, *Scripta Mater.*, 2000, **43**, p 743–749
36. A. Belyakov, Y. Kimura, and K. Tsuzaki, Microstructure Evolution in Dual Phase Stainless Steel During Severe Deformation, *Acta Mater.*, 2006, **54**, p 2521–2532
37. M. Topic, C. Allen, and R. Tait, The Effect of Cold Work and Heat Treatment on the Fatigue Behavior of 3Cr12 Corrosion-Resistant Steel Wire, *Int. J. Fatigue*, 2007, **29**, p 49–56
38. H.W. Hayden and S. Floreen, The Influence of Martensite and Ferrite on the Properties of Two Phase Stainless Steels Having Microduplex Microstructures, *Metall. Trans.*, 1950, **1**, p 1955–1959
39. R.N. Wright and J.R. Wood, Fe-Cr-Mn Micro-Duplex Ferritic Martensitic Stainless Steels, *Metall. Trans.*, 1977, **8A**, p 1977–2007